Sn-Doped TiO2 Photoanode for Dye-Sensitized Solar Cells

ARTICLE *in* THE JOURNAL OF PHYSICAL CHEMISTRY C · APRIL 2012

Impact Factor: 4.77 · DOI: 10.1021/jp212517k

7 AUTHORS, INCLUDING:

Yandong Duan
Chinese Academy of Sciences
39 PUBLICATIONS **609** CITATIONS
SEE PROFILE

Nianqing Fu
Chinese Academy of Sciences
18 PUBLICATIONS **207** CITATIONS
SEE PROFILE

Jingbo Zhang
Chinese Academy of Sciences
38 PUBLICATIONS **859** CITATIONS
SEE PROFILE

Yuan Lin
Chinese Academy of Sciences
193 PUBLICATIONS **2,163** CITATIONS
SEE PROFILE

THE JOURNAL OF PHYSICAL CHEMISTRY C

Article

pubs.acs.org/JPCC

Sn-Doped TiO_2 Photoanode for Dye-Sensitized Solar Cells

Yandong Duan,[†,‡] Nianqing Fu,[†,‡] Qiuping Liu,[§] Yanyan Fang,[†,‡] Xiaowen Zhou,[†] Jingbo Zhang,[†] and Yuan Lin[†,*]

[†]Beijing National Laboratory for Molecular Sciences, Key Laboratory of Photochemistry, Institute of Chemistry, Chinese Academy of Sciences, Beijing 100190, China

[‡]Graduate School of Chinese Academy of Sciences, Beijing 100049, China

[§]School of Mechanical, Electronic and Control Engineering, Beijing Jiaotong University, Beijing 100044, China

Supporting Information

ABSTRACT: A series of Sn-doped TiO_2 with Sn content ranging from 0.25 to 1 mol % were successfully synthesized by the hydrothermal method, and its performance as the photoanode of dye-sensitized solar cells (DSSCs) was investigated. TEM and XRD results indicate that the doping has no effect on the morphology and the crystal form of TiO_2. The shift of XRD peaks observed at higher angle and the XPS results indicate Sn^{4+} ions incorporation into the TiO_2 lattice. The flatband potential of Sn-TiO_2 films shifts from −0.505 V (vs SCE) to −0.55 V with increasing Sn content from 0 to 1 mol at. %, which is beneficial to the increase of V_{oc}. The higher transfer rate of electrons in the Sn-doped TiO_2 films than in the undoped TiO_2 films is confirmed by IMPS measurements, which is favorable to the higher J_{sc}. IMVS and EIS measurements indicate that the charge recombination increases with increasing Sn doping content. Taking these factors, the optimum efficiency of 8.31% was found at 0.5 mol % Sn-doped TiO_2 based DSSCs, which gave an efficiency improved by 12.1% compared with that of the cells based on pure TiO_2 (7.45%). This work shows that Sn-doped TiO_2 is a most interesting material and has good potential for application in photoenergy conversion devices.

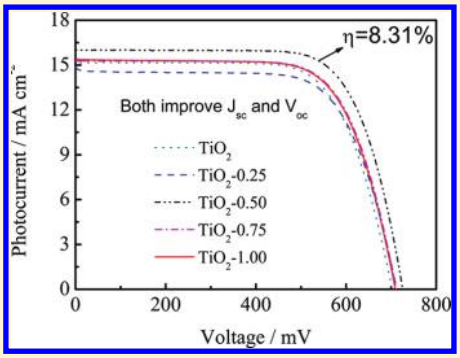

1. INTRODUCTION

Dye-sensitized solar cells (DSSCs) have become an attractive alternative to conventional silicon-based solar cells due to their relatively high energy conversion efficiency and low cost.[1−3] Many semiconductors have been studied for using as photoanode materials to develop high performance DSSCs, such as TiO_2,[4] ZnO,[5] SnO_2,[6] Nb_2O_5,[7] and $SrTiO_3$[8] et al. Apparently, TiO_2 has been proven to be the best semiconductor electrode material due to its chemical stability and excellent charge transport capability. The photoelectric conversion efficiency (η) of DSSCs has reached greater than 11% using anatase TiO_2 as the photoanode materials.[4] The mesoscopic TiO_2 film is at the heart of all these devices, playing a fundamental role for the DSSCs performance in light energy conversion. In DSSCs, the TiO_2 bears three major roles, (i) providing a substrate for dye adsorption, (ii) accepting electrons from the dye's excited state, and (iii) transporting the electron toward the FTO.

Doping TiO_2 with metal or nonmetal ions has been considered as a promising way to improve the properties of TiO_2 photoanode. To improve the IPCE and J_{sc}, many efforts have been made to enhance the charge collection efficiency, such as improving the charge transport[9,10] or suppressing the recombination.[11−13] However, due to the positive shifting of the conduction band (CB) of TiO_2 in these works, the V_{oc} of the DCCSs could decrease. Another way to improve the J_{sc} of DSSCs is to modify the surface structure of the TiO_2, so that the TiO_2 could adsorb more dye. Zhang et al.[14] have found that La-doping could improve the efficiency of DSSCs. The improvement was ascribed to more dye absorbed on the surface of TiO_2 due to the increasing of the oxygen vacancy density on the TiO_2 surface. There is also a few work on the improvement of V_{oc} to increase the efficiency of DSSCs. Feng et al.[15] prepared Ta-doped TiO_2 nanowire arrays for DSSCs and they were found to achieve a very high open-circuit voltage of 0.87 V due to the negative shifting of the CB of TiO_2, close to the theroretical maximum. Although extensive studies have been made on doping TiO_2, none of which could both enhance the short-circuit current density and open-circuit voltage.

In this paper, Sn-doped TiO_2 was synthesized by hydrothermal method. The doping of Sn in the TiO_2 lattice was confirmed by X-ray powder diffraction (XRD) and X-ray photoelectron spectroscopy (XPS). The Sn-doped TiO_2 nanoparticles were successfully applied as the photoanode material in DSSCs, and they were found to improve the open-circuit voltage due to the negative shift of V_{fb} of TiO_2 and enhance the short circuit current density due to the faster electron transport in the Sn-doped TiO_2 films.

Received: December 28, 2011
Revised: April 8, 2012
Published: April 9, 2012

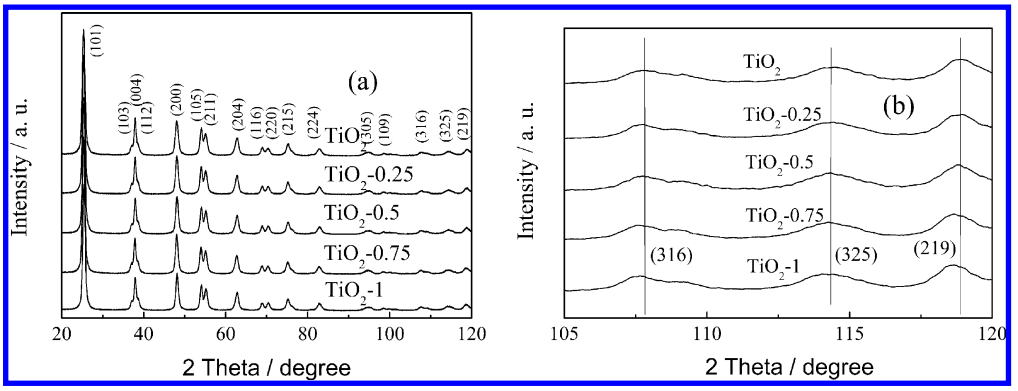

Figure 1. (a) XRD patterns of the TiO_2 and Sn-doped TiO_2. (b) Magnification of the anatase (316), (325), and (219) peaks of the samples.

2. EXPERIMENTAL SECTION

2.1. Materials. Tetrabutyl titanate (99%, Acros, Belgium), butanol (Beijing Chemical Works), acetic acid (Beijing Chemical Works), tin(IV) *tert*-butoxide (99.9%, Alfa), tin(IV) chloride (anhydrous, 99%, Sinopharm Chemical Reagent Co., Ltd.), 3-methoxypropionitrile (MPN, 99%, GC, Alfa), LiI (AR, Acros), I_2 (AR, Acros), and 4-*tert*-butylpyridine (TBP, AR, Aldrich) were commercially available and used without further purification. 3-Hexyl-1-methylimidazolium iodide (HMII) was prepared according to the literature.[16]

2.2. Synthesis of TiO_2 and Sn-Doped TiO_2. Both TiO_2 and Sn-doped TiO_2 were synthesized by using the hydrothermal method.[9] Tetrabutyl titanate (10 mL), butanol (60 mL), acetone (10 mL), and acetic acid (10 mL) were mixed. A mixture of butanol (40 mL) and distilled water (3 mL) was then added to the above solution. After being stirred continuously for 1 h, the mixture was transferred into an autoclave for the hydrothermal process at 240 °C for 6 h. After being cooled to room temperature, the concentrated colloid contained 13% TiO_2. For preparing of the Sn-doped samples, tin(IV) *tert*-butoxide was added to the tetrabutyl titanate (molar ratio of Sn and Ti were 0.25:100, 0.5:100, 0.75:100, 1:100) to start the hydrolysis reaction. The obtained samples using tin(IV) *tert*-butoxide was denoted as TiO_2-0.25, TiO_2-0.5, TiO_2-0.75, TiO_2-1.

2.3. Cell Fabrication and Photovoltaic Measurements. TiO_2 and Sn-doped TiO_2 films (ca. 11 μm) were fabricated on the FTO substrates (fluorine-doped SnO_2, 15 Ω/sq) using a doctor-blade method and the electrodes were heated at 450 °C for 30 min. After the sintering, when the temperature cooled to about 90 °C, the electrodes were immersed in a dye bath containing 0.5 mM *cis*-$Ru(H_2dcbpy)_2(NCS)_2$(H_2dcbpy = 4,4′-dicarboxy-2,2′-bipyridyl) (N3) in ethanol for 24 h. The film thickness was measured by CCD laser displacement sensor (Keyence Corp.). The redox electrolyte was a mixture of 0.5 M LiI, 0.05 M I_2, 0.6 M TBP, and 0.6 M HMII in MPN. The counter electrode was Pt-coated FTO.

The photocurrent density−voltage (J−V) measurement was tested using a Keithly 2611 Source Meter (Keithley Instruments, Inc.). The light source was a AM 1.5 solar simulator (91160A, Newport Co.). The incident light intensity was 100 mW cm^{-2} calibrated with a standard Si solar cell. The tested solar cells were masked to a working area of 0.2 cm^2.

2.4. Characterization. The X-ray diffraction (WAXRD, 20−90°) were obtained by D/MAX-2500 diffractometer (Rigaku Co.) with Cu Kα radiation (k = 0.154 06 nm) operated at 40 kV and 150 mA. The data for Rietveld analysis were collected in the 2θ range 20−120° with a step size of 0.02°. The high resolution transmission electron microscopy (HRTEM) was performed with an JEM2010 transmission electron microscope operated at 200 kV. X-ray photoelectron spectroscopy (XPS) were performed to measure the surface elements and the chemical state. The binding energies are calibrated by C1s photoelectron peak (284.6 eV).

Mott−Schottky analysis was performed in a three-electrode cell in the dark. TiO_2 or Sn-doped TiO_2 single films without dyes (ca. 3 μm) were used as the electrode, a saturated calomel electrode (SCE) served as the reference electrode, and platinum wire was used as the counter electrode. The active area was 0.25 cm^2. TiO_2 or Sn-doped TiO_2 films (ca. 4 μm) absorbed by dyes were used for the EIS, IMPS, and IMVS test. Electrochemical impedance spectroscopy (EIS) data were obtained under 100 mW cm^{-2} illuminations, using a perturbation of ±10 mV over the open-circuit potential by using Solartron 1255B frequency analyzer and Solartron SI 1287 electrochemical interface system. IMPS and IMVS were performed using a green light emitting diode (max = 520 nm) driven by a solartron 1255B frequency-response analyzer. The LED provided both the dc and ac components of the illumination.

3. RESULTS AND DISCUSSION

3.1. X-ray Diffraction and HRTEM Analysis. Figure 1a shows the X-ray diffraction patterns of the TiO_2 and TiO_2 with different degrees of Sn-doping. All peaks can be indexed to the anatase phase (JCPDS No. 89-4921). The crystallite size was estimated with Scherrer equation. From the full width at half-maximum of the strongest anatase diffraction (101), the crystallite size was calculated to be ca. 14 nm for both TiO_2 and Sn-doped TiO_2 samples.

According to the XRD patterns, the anatase crystal structure and the particle size were not noticeably influenced by the Sn-doping. As can be seen in Figure 1b, the diffraction peaks shift to lower theta values with increasing Sn content because of the larger effective radius of Sn^{4+} (0.69 Å) compared to that of Ti^{4+} (0.61 Å), in accordance with the Bragg equation: $2d \sin \theta = \lambda$. And this effect is more obvious in the higher theta.

The XRD diffraction data were fitted using the Rietveld powder diffraction profile fitting technique.[11] The fitted results are shown in Figure S1 and Table 1. It can be seen that the final fitting parameters, profile factor R_p, weighted profile factor R_{wp} and goodness of fit indicator s are satisfactory. As shown in Figure 2, the linear evolution of the lattice cell parameters as a function of the Sn content verifies Vegard's law.[17] The lattice

dx.doi.org/10.1021/jp212517k | J. Phys. Chem. C 2012, 116, 8888−8893

Table 1. Rietveld Fitted Results of the XRD Patterns[a]

	R_p (%)	R_{wp} (%)	S	a (Å)	c (Å)	V (Å^3)
TiO_2	9.4	11.4	1.691	3.7807	9.4904	135.6367
TiO_2−Sn-0.25	10.3	12.0	1.848	3.7808	9.4927	135.6999
TiO_2−Sn-0.5	9.57	11.6	1.844	3.7809	9.4944	135.7266
TiO_2−Sn-0.75	9.06	11.1	1.696	3.7811	9.4971	135.7820
TiO_2−Sn-1	9.40	11.4	1.674	3.7814	9.5013	135.8616

[a]Here R_p, R_{wp}, and s are the profile factor, the weighted profile factor, and the goodness of fit indicator, respectively. a and c are the lattice parameters.

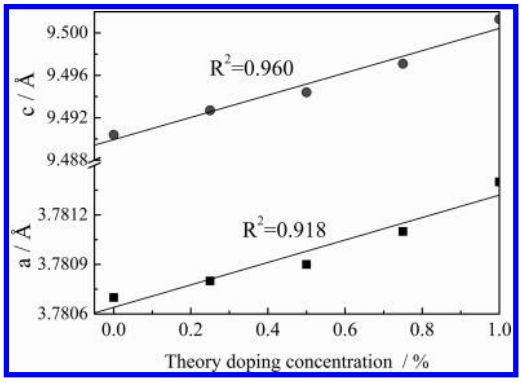

Figure 2. Variation of the cell parameters as a function of the doping concentration.

parameters increase when the concentration of the dopant increases. Although the change is very small, the concentration of the dopant plays a role in the variation of lattice parameters that gives an indication for the Ti substituting in the TiO_2 crystalline structure.

Figure 3 shows the particle size and morphology of TiO_2 and Sn-doped TiO_2 samples. It can be found that the mean sizes of

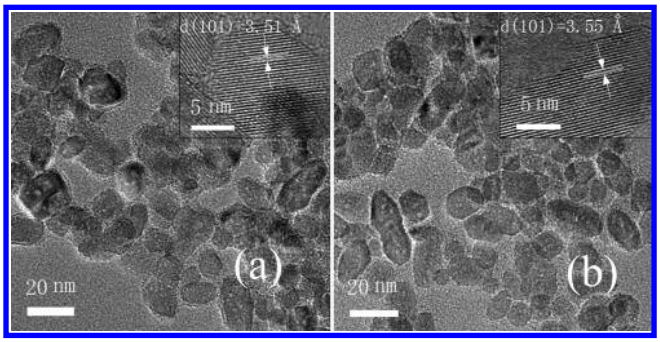

Figure 3. HRTEM images for the TiO_2 (a) and 1% Sn-doped TiO_2 (b) nanoparticles.

TiO_2 and Sn-TiO_2 was about 14 nm, which is in accordance with the XRD results. The HRTEM images of TiO_2 and TiO_2-1 are shown in the inset of Figure 3a,b. The corresponding lattice fringes were clearly observed, indicating that TiO_2 nanoparticles formed with good crystallinity. The interplanar spacing was determined to be 3.51 Å for the TiO_2 and 3.55 Å for the TiO_2-1, corresponding to the (101) crystal face in the anatase phase, and this result further confirms the substitution of Ti^{4+} by Sn^{4+}.

3.2. XPS Analysis. XPS, as a surface sensitive technique, was used to confirm the presence and chemical states of Ti, Sn, and O in our samples. Figure 4a shows the Ti2p XPS spectra of

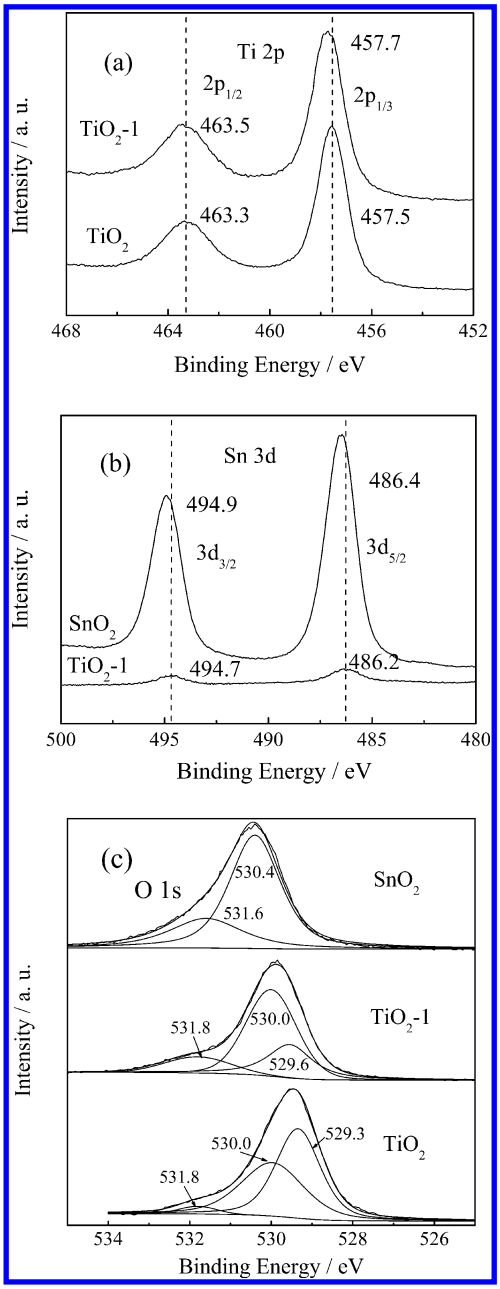

Figure 4. XPS spectra of Ti, Sn, and O for the TiO_2, Sn-TiO_2, and SnO_2 samples.

the TiO_2 and TiO_2-1 samples. The two peaks of the Ti2p spectra for the TiO_2-1 show a slight positive shift comparing with the spectra for pure TiO_2, which is likely attributed to the interaction between titanium atoms, oxygen atoms and Sn atoms. Consistent with this, the Sn 3d spectrum of TiO_2-1 reveals a negative shift of 0.2 eV toward lower binding energy compared to those of SnO_2 (Figure 4b). This can be attributed to the variation in electronegativities of the Ti and Sn elements (Ti = 1.54, Sn = 1.96).[18] These observations confirm the formation of Ti−O−Sn structure in the Sn-doped TiO_2, owing to the substitution of Ti by Sn.

dx.doi.org/10.1021/jp212517k | J. Phys. Chem. C 2012, 116, 8888−8893

As shown in Figure 4c, the O 1s spectrum for TiO_2 can be deconvoluted to three peaks. The large peak at 529.3 eV is assigned to lattice oxygen in anatase TiO_2, whereas the two peaks located at 530.0 and 531.8 eV could be attributed to surface bridging O atoms and hydroxyl O atoms, respectively.[19,20] In sample SnO_2, the characteristic peak at 530.4 eV is also assigned to lattice oxygen in SnO_2, whereas the other peak positioned at 531.6 should be ascribed to surface hydroxyl groups Sn−OH. In the TiO_2-1 sample, the binding energy of the lattice oxygen is located at 530.1 eV, which is between 529.8 (TiO_2) and 530.8 eV (SnO_2), owing to the variation in electronegativities of the two metal elements. The remaining two O 1s peaks of TiO_2-1 at 530.0 and 531.8 eV are attributed to the same chemical constituents as those assigned for the pure phase TiO_2. The atomic concentration is calculated by using Avantage3.95 software, and the results are shown in Table S1. The molar ratio of Sn to Ti on the Sn-TiO_2 surface is in good agreement with the theoretical value in Sn and Ti sources.

3.3. Effect of Sn^{4+} Doping on the Conduction Band Edge Shift. The flat band potential (E_{fb}) of the electrode material in a DSSCs is very important, because the V_{oc} is determined by the difference between the red-ox potential of the electrolyte and E_{fb}.[21,22] The E_{fb} and donor density of the TiO_2 and Sn-doped TiO_2 films were obtained from Mott−Schottky (MS) measurements. $1/C^2 = (2/A^2 e\varepsilon\varepsilon_0 N_D)(E - E_{fb} - KT/e)$, where C represents the capacitance of the space charge region, ε_0 is the vacuum permittivity, ε is the dielectric constant of the TiO_2 layer, e is the electron charge, E is the applied potential, E_{fb} is the flat band potential, k is the Boltzmann constant, T is the absolute temperature, N_D is the donor density, and A is the active surface.[23] The intercept of the fitted lines are E_{fb}, and the slope of the fitted lines are used to calculate the donor density. As shown in Figure 5, the E_{fb}

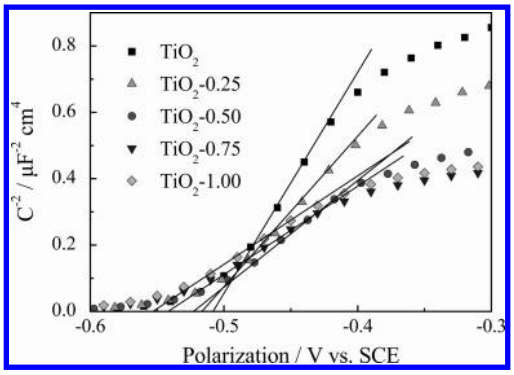

Figure 5. Mott−Schottky plots for TiO_2 and Sn-doped TiO_2 films.

was negatively shifted with increasing the doping amount. A negative shift of E_{fb} in this plot means a shift away from the red-ox potential, thereby an increment of V_{oc}, and the results are shown in Table 2. The calculated donor density increases with the molar ratio of Sn/Ti increases.

3.4. Photovoltaic Performance. Figure 6 shows the current density−voltage curves of the open cells based on TiO_2 and Sn-doped TiO_2 photoelectrodes. The average performance characteristics obtained from multiple cells with the same Sn content are summarized in Table 3. The short-circuit photocurrent density (J_{sc}), the open-circuit voltage and the photoelectric conversion efficiency increase with the Sn-doping to reach a maximum at a Sn/Ti ratio of 0.5 at % and then decrease. The film thinkness and dye-loading amount are

Table 2. Flat Band Potential (E_{fb}) and Donor Density (N_d) of TiO_2 and the Sn-Doped TiO_2 Films

samples	E_{fb}/V vs SCE	N_d ($\times 10^{19}$)/cm^{-3}
TiO_2	−0.505	0.87
TiO_2-0.25	−0.514	1.08
TiO_2-0.50	−0.523	1.80
TiO_2-0.75	−0.539	2.14
TiO_2-1.00	−0.550	2.18

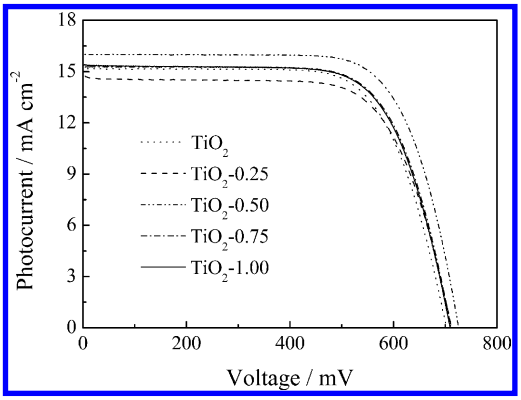

Figure 6. Current density−voltage ($J-V$) curves of DSSCs.

Table 3. Photovoltaic Properties of DSSCs Assembled with TiO_2 Films of Different Sn Contents

	J_{SC} (mA cm^{-2})	V_{OC} (mV)	η (%)	FF	dye loading ($\times 10^{-7}$ mol cm^{-2})	film thickness (μm)
TiO_2	15.15	695	7.45	0.707	0.95	10.6
TiO_2-0.25	15.27	711	7.68	0.719	1.01	10.8
TiO_2-0.5	16.01	722	8.31	0.707	0.98	10.6
TiO_2-0.75	15.41	710	7.64	0.699	0.93	10.9
TiO_2-1	14.85	709	7.26	0.688	1.05	10.7

similar for both of the photoanode films, indicating that the increase of photocurrent for the Sn-doped TiO_2 is not due to the increase of the dye absorption. The higher J_{sc} should result from the enhanced electron transport in the TiO_2 films, which could be explained in the IMPS analysis part. The higher V_{oc} should result from the elevated E_{fb}. With the doping content increases, the concentration of impurities increases. These impurities could act as charge trapping site for the electron−hole recombination. And more serious recombination at high doping content (>0.5 at%) could results in a smaller V_{oc} and J_{sc}.

3.5. IMPS and IMVS Analysis of DSSCs. IMPS and IMVS were used to investigate further the electron transport and recombination processes.[23,24] The IMPS and IMVS plots display a semicircle in the complex plane. The electron transport time (τ_d) and the electron lifetime (τ_n) can be estimated from the $\tau = (2\pi f_{min})^{-1}$, where f_{min} is the bottom of the semicircle at the IMPS and the IMVS plots respectively. Figures 7 and 8 show complex plane plots of the IMPS and IMVS spectrum for the TiO_2 and Sn-doped TiO_2 thin films and the inset show the time constant τ_d and τ_n. The electron transport time constants (τ_d) for the Sn-doped TiO_2 films decrease with the increasing of Sn/Ti ratio. And a shorter electron transport time indicates a higher electron transport rate in the TiO_2 film. The reason that the Sn-doped TiO_2 thin

dx.doi.org/10.1021/jp212517k | J. Phys. Chem. C 2012, 116, 8888−8893

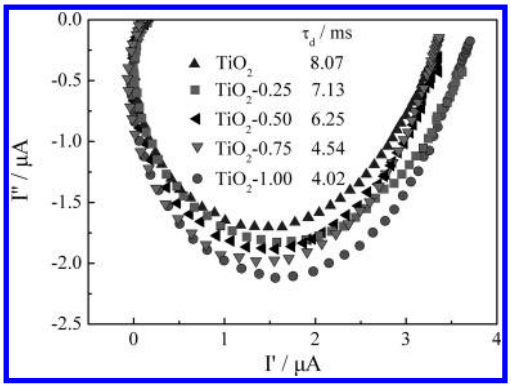

Figure 7. Complex plane plots of the TiO_2 and the Sn-doped TiO_2 DSSCs obtained from IMPS measurements.

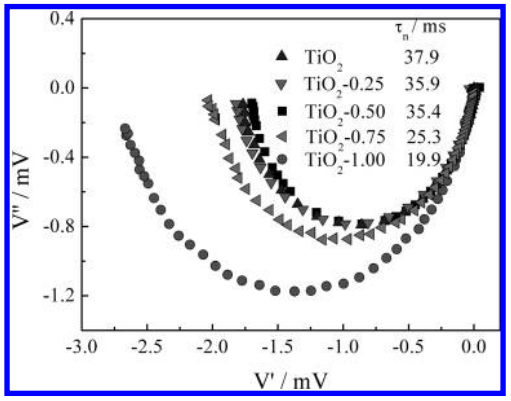

Figure 8. Complex plane plots of the TiO_2 and the Sn-doped TiO_2 DSSCs obtained from IMVS measurements.

film has faster electron transport in the film may be related to the increased electron density. The electron lifetime constants (τ_n) for the Sn-doped TiO_2 films also decrease with the increasing of Sn/Ti ratio. The shorter electron lifetime indicate that more recombination sites exist in Sn-TiO_2 films than in TiO_2 film due to the doping. And fast recombination rate could be the main reason for the decreasing of V_{oc} at high Sn/Ti ratio (>0.5 mol %). The charge collection efficiency (η_{cc}) of DSSCs is determined by the relation: $\eta_{cc} = 1 - (\tau_d/\tau_n)$. η_{cc} is a measure of the percent of photoinjected electrons that reach the electron collector without recombining with either the oxidized dye or oxidized component in the redox electrolyte. The obtained η_{cc} value for TiO_2, TiO_2-0.25, TiO_2-0.5, TiO_2-0.75, and TiO_2-1 were 78.7%, 80.1%, 82.3%, 82.0%, and 79.7%, respectively. This result is in accordance with the tendency of short-circuit photocurrent density variation. At low doping content (≤0.5 mol %), faster electron transport results in the increasing of the J_{sc}. At high doping content(>0.5 mol %), the recombination is the main factor that affects the J_{sc}, and the serious recombination results in the decreasing of the J_{sc}.

3.6. Electrochemical Impedance Spectrascopic Analysis. EIS technique has been widely employed to investigate the kinetics of electrochemical and photoelectrochemical process occurring in DSSCs.[25−28] As illustrated in Figure 9, the impedance spectra of DSSCs based on TiO_2 and Sn-doped TiO_2 films were measured ranging from 1 Hz to 100 kHz. Two semicircles, including a small semicircle at high frequency and a large one at low frequency, were observed in the Nyquist plots of EIS spectra (Figure 9). As shown in Figure 9, the small semicircle in the frequency range (<10 Ω) fitted to a charge

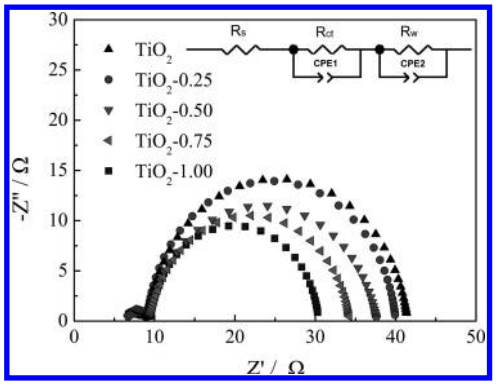

Figure 9. EIS specra of the TiO_2 and the Sn-doped TiO_2 DSSCs. The inset of EIS plots represents the equivalent circuit for EIS.

transfer resistance (R_{ct}) and the Helmholtz capacitance ($C_{\mu 1}$) should be ascribed to the charge transfer at the interfaces of the redox electrolyte/Pt counter electrode. The large semicircle in the low-frequency region fitted to a transport resistance (R_w) and the Helmholtz capacitance ($C_{\mu 2}$) is related to the charge transfer across either the TiO_2/redox electrolyte interface or the FTO/TiO_2 interface. According to the EIS model reported in the literature,[29] the fitted parameters including R_{ct} and R_w obtained by Zview software are exhibited in Table 4. Under

Table 4. R_{ct}, R_w, the Mean Electron Lifetme (τ_e),and the Helmholtz Capacitance ($C_{\mu 2}$) of the TiO_2 and Sn-Doped TiO_2 Fims Determined by Electrochemical Impedance Spectroscopy Measurement

samples	R_{ct}	R_w	$C_{\mu 2}/\mu$F
TiO_2	4.8	32.3	50.7
TiO_2-0.25	4.4	30.1	45.5
TiO_2-0.50	3.5	28.4	35.6
TiO_2-0.75	3.2	24.1	32.5
TiO_2-1.00	3.2	20.8	25.5

open circuit condition, no current passes through the external circuit, and the electrons injected into TiO_2 or Sn-doped TiO_2 are recombined by redox electrolyte at the TiO_2/dye/electrolyte interface. The increased charge recombination found for the Sn-doped TiO_2 cell could be attributed to higher concentration impurities due to the doping, which acts as a charge trapping site for the electron−hole recombination, hence leading to the decreasing of photon-to-electron conversion efficiency at high Sn content (>0.5 mol %). Table 4 also shows the Helmholtz capacitance ($C_{\mu 2}$) produced by the accumulation of electrons in the TiO_2 film. This Helmholtz capacitance describes the change of electron density under a small variation of the Fermi level. Thus, the value of $C_{\mu 2}$ gives the total density of free electrons in the TiO_2 conduction band and localized electrons in the trap states. The Sn-doped TiO_2 film had a smaller capacitance value than the pure-TiO_2 film,[30] which results from the fact that less photogenerated electrons are captured by the empty trap states in the Sn-doped film due to doping, and this result favors the electron transport.

4. CONCLUSION

In summary, the Sn-doped TiO_2 were successfully prepared by hydrothermal method under optimized Sn content. The best efficiency of 8.31% was achieved by DSSCs with 0.5 mol % Sn-doped TiO_2, which gave an efficiency improved by 12.1%

dx.doi.org/10.1021/jp212517k | J. Phys. Chem. C 2012, 116, 8888−8893

compared with that of the cells based on pure TiO_2. The DSSCs with Sn-doped TiO_2 were found to improve the open-circuit voltage due to the negative shift of V_{fb} of TiO_2 and enhance the short circuit current density due to the faster electron transport in the Sn-doped TiO_2 films. IMVS and EIS measurement indicate that the increased charge recombination found for the Sn-doped TiO_2 cell could be attributed to high-concentration impurities due to the doping, which acts as charge trapping site for the electron−hole recombination, hence leading to the decreasing of photon-to-electron conversion efficiency at high Sn content (>0.5 mol %). These findings pave a new way to tune the band structure of TiO_2 and improve the charge transport for the high performance of DSSCs. Therefore, Sn-doped TiO_2 may be developed as a promising photoelectrode material for high-efficiency DSSCs and other phothoenergy conversion devices.

■ ASSOCIATED CONTENT

Supporting Information

Figure of the Rietveld fitted results. Sn content in the TiO_2 nanoparticles determined using XPS. This information is available free of charge via the Internet at http://pubs.acs.org.

■ AUTHOR INFORMATION

Corresponding Author

*E-mail: linyuan@iccas.ac.cn. Tel: 86-10-82615031. Fax: 86-10-82617315.

Notes

The authors declare no competing financial interest.

■ ACKNOWLEDGMENTS

This work was supported by the National Natural Science Foundation of China (20973183) and National Research Fund for Fundamental Key Project (2012CB932900).

■ REFERENCES

(1) Wei, D. *Int. J. Mol. Sci.* **2010**, *11* (3), 1103−1113.
(2) O'Regan, B. C.; Durrant, J. R. *Acc. Chem. Res.* **2009**, *42* (11), 1799−1808.
(3) Hagfeldt, A.; Boschloo, G.; Sun, L.; Kloo, L.; Pettersson, H. *Chem. Rev.* **2010**, 6595−6663.
(4) Nazeeruddin, M. K.; De Angelis, F.; Fantacci, S.; Selloni, A.; Viscardi, G.; Liska, P.; Ito, S.; Takeru, B.; Grätzel, M. *J. Am. Chem. Soc.* **2005**, *127* (48), 16835−16847.
(5) Jensen, R. A.; Van Ryswyk, H.; She, C. X.; Szarko, J. M.; Chen, L. X.; Hupp, J. T. *Langmuir* **2010**, *26* (3), 1401−1404.
(6) Snaith, H. J.; Ducati, C. *Nano lett.* **2010**, *10* (4), 1259−1265.
(7) Hara, K.; Horiguchi, T.; Kinoshita, T.; Sayama, K.; Sugihara, H.; Arakawa, H. *Sol. Energy Mater. Sol. Cells* **2000**, *64* (2), 115−134.
(8) Yang, S. M.; Kou, H. Z.; Wang, H. J.; Cheng, K.; Wang, J. C. *J. Phys. Chem. C* **2010**, *114* (2), 815−819.
(9) Liu, J.; Yang, H.; Tan, W.; Zhou, X.; Lin, Y. *Electrochim. Acta* **2010**, *56* (1), 396−400.
(10) Lv, X.; Mou, X.; Wu, J.; Zhang, D.; Zhang, L.; Huang, F.; Xu, F.; Huang, S. *Adv. Funct. Mater.* **2010**, *20* (3), 509−515.
(11) Chandiran, A. K.; Sauvage, F. d. r.; Casas-Cabanas, M.; Comte, P.; Zakeeruddin, S. M.; Graetzel, M. *J. Phys. Chem. C* **2010**, *114* (37), 15849−15856.
(12) Zhang, X.; Liu, F.; Huang, Q.-L.; Zhou, G.; Wang, Z.-S. *J. Phys. Chem. C* **2011**, *115* (25), 12665−12671.
(13) Ko, K. H.; Lee, Y. C.; Jung, Y. J. *J. Colloid Interface Sci.* **2005**, *283* (2), 482−487.
(14) Zhang, J.; Zhao, Z.; Wang, X.; Yu, T.; Guan, J.; Yu, Z.; Li, Z.; Zou, Z. *J. Phys. Chem. C* **2010**, 18396−18400.
(15) Feng, X. J.; Shankar, K.; Paulose, M.; Grimes, C. A. *Angew. Chem., Int. Ed.* **2009**, *48* (43), 8095−8098.
(16) Bonhôte, P.; Dias, A.-P.; Papageorgiou, N.; Kalyanasundaram, K.; Grätzel, M. *Inorg. Chem.* **1996**, *35* (5), 1168−1178.
(17) Denton, A. R.; Ashcroft, N. W. *Phys. Rev. A* **1991**, *44*, 1219−1227.
(18) Li, J.; Zeng, H. C. *J. Am. Chem. Soc.* **2007**, *129* (51), 15839−15847.
(19) Xu, H.; Zhang, L. *J. Phys. Chem. C* **2010**, *114* (26), 11534−11541.
(20) Bullock, E. L.; Patthey, L.; Steinemann, S. G. *Surf. Sci.* **1996**, *352*−*354* (0), 504−510.
(21) Bandara, J.; Pradeep, U. W. *Thin Solid Films* **2008**, *517* (2), 952−956.
(22) Radecka, M.; Rekas, M.; Trenczek-Zajac, A.; Zakrzewska, K. *J. Power Sources* **2008**, *181* (1), 46−55.
(23) Zhang, W.-D.; Jiang, L.-C.; Ye, J.-S. *J. Phys. Chem. C* **2009**, *113* (36), 16247−16253.
(24) Zhu, K.; Jang, S.-R.; Frank, A. J. *J. Phys. Chem. Lett.* **2011**, *2* (9), 1070−1076.
(25) Zheng, Q.; Kang, H.; Yun, J.; Lee, J.; Park, J. H.; Baik, S. *ACS Nano* **2011**, *5* (6), 5088−5093.
(26) Bisquert, J.; Mora-Seró, I. N. *J. Phys. Chem. Lett.* **2009**, *1* (1), 450−456.
(27) Bisquert, J. *Phys. Chem. Chem. Phys.* **2003**, *5* (24), 5360−5364.
(28) Andersen, A. R.; Halme, J.; Lund, T.; Asghar, M. I.; Nguyen, P. T.; Miettunen, K.; Kemppainen, E.; Albrektsen, O. *J. Phys. Chem. C* **2007**, *115* (31), 15598−15606.
(29) Wang, S.; Zhang, J.; Chen, S.; Yang, H.; Lin, Y.; Xiao, X.; Zhou, X.; Li, X. *Electrochim. Acta* **2011**, *56* (17), 6184−6188.
(30) Wang, K.-P.; Teng, H. *Phys. Chem. Chem. Phys.* **2009**, *11* (41), 9489−9496.